

KINEMATIC MEASUREMENTS OF GAS AND STARS IN SPIRAL GALAXIES

JOHN E. BECKMAN

Instituto de Astrofísica de Canarias, E-38200 La Laguna, SPAIN

Consejo Superior de Investigaciones Científicas, SPAIN

ALMUDENA ZURITA

Isaac Newton Group of Telescopes, E-38700 S.C. de La Palma, SPAIN

JUAN C. VEGA BELTRÁN

Departamento de Física, Universidad de La Laguna, E-38200 La Laguna, SPAIN

Instituto de Astrofísica de Canarias, E-38200 La Laguna, SPAIN

Abstract: In this article we first give a brief, historically based, survey of kinematic observations, essentially of rotation curves of spiral galaxies, produced as techniques have advanced and new wavelength ranges have opened up. We then describe the basic inferences from kinematic measurements relevant to galactic structure: the rotational velocity and the velocity dispersion in gas and stars, and how these are made. This is followed by a selection of observations of individual galaxies, picked to illustrate how structural components: bulges, discs, lenses and bars, can be detected and analyzed kinematically as a complement to, or even a substitute for surface photometry. A further section shows how two dimensional kinematic observations of galaxies are even more powerful than one dimensional long-slit optical observations. This is illustrated by Fabry–Pérot mapping of NGC 1530 in $H\alpha$, from which we can clearly detect streaming motions in the arms, high velocity flows on either sides of the bar, and inward spiralling gas flow towards the nucleus, and from which we can also relate velocity gradient behaviour with the enhancement or the inhibition of the star formation rate. Finally we explain how continued technical improvement will ensure continued progress in this mature but rewarding field.

1 Basic galactic kinematics: observational method

The fact that galaxies rotate on their axes was discovered in 1914 by [1] from the curved shapes of long slit spectra of M81 and M104. The first rotation curve of a galaxy was obtained in 1918 by [2] for the central part of the Andromeda nebula, M31, with photographic spectroscopy which needed 80 hours of exposure time! The classical piece of work on the rotation curve of M31 by [3] using emission spectra from

44 HII regions in the central zone of the galaxy and 4 towards the outside, required a total of 292 hours of photographic exposure. Small wonder that real progress in using kinematic measurements to investigate the internal dynamics of galaxies had to await the introduction of modern techniques on large telescopes. Even as late as 1970 Rubin and Ford's M31 rotation curve ([4]) containing 67 independent data points, was based on 112 hours of observations. The first major step came with the use of image tubes; a long slit spectrum of M31 of quality sufficient to obtain a good major axis rotation curve was possible on the Lick 3.5 m telescope in ~ 20 hours during the 1970's and early 80's. Since then there have been three major advances in optical rotation curve observing: the use of CCD's, the use of larger telescopes, and the use of Fabry-Pérot interferometry to obtain radial velocity maps in emission lines over the full face of a galaxy in times of order 3 hours on a 4m telescope.

Complementary rotational kinematic information can be obtained using neutral gas, in either atomic (HI) or molecular (H_2) form. The first rotation curve for an external galaxy using HI was obtained by [5], again for M31, and even in this pioneering measurement they showed that the curve in HI could be measured out to at least twice as far from the galactic centre as the stellar population. The use of HI gives far greater cover of a typical galaxy disc than that of optical emission lines, but suffers from poor angular resolution. One can reach arcsecond resolution with the VLA, but the exposure times reach tens of hours for a field of a few arcminutes, and all other telescopes give poorer resolution. The key molecule for cold gas observations is CO, and with modern millimetre wave interferometers one can go to a couple of arcsec resolution. The first rotation curve in CO was published for the Milky Way by [6]. Here too however exposure times are still rather long, and the number of galaxies observed in this way is limited. We should point out that in terms of the material sampled, HII, HI and CO (which represents H_2) cover the main phases of the interstellar medium (ISM) and in terms of physical information are complementary. In terms of kinematic information if all are available they can normally be used in parallel, because kinematically the three types of hydrogen behave essentially equally, but the coverage of the disc is also complementary. To simplify a little, H_2 (CO) samples well the centres of most disc galaxies, and their spiral arms, HI samples the whole disc out to large radii, but often with a "hole" in the centre, while HII (via $H\alpha$) samples star forming regions, with high precision but with incomplete bulge, bar and disc cover. The other way to map a galaxy kinematically is, of course via its stellar population. Stellar lines give intrinsically less precise velocities because they are broader and the stellar population often has a high velocity dispersion. We will see below that the kinematic behaviour of gas and stars can be different, and this gives us interesting information about the structural evolution of the galaxy.

2 Velocity fields and their broad interpretation

To first order it is found, from a distillation of much observational material, that disc galaxies are essentially in concentric circular rotation in a plane about a central axis. The velocity of this rotation varies with radius from the galactic centre, and is determined by the radial distribution of mass within the galaxy. The plot of circular velocity v_r versus galactocentric radius r (normally called the “rotation curve”) is observed to be divisible into two regimes: a rapidly rising regime from the centre

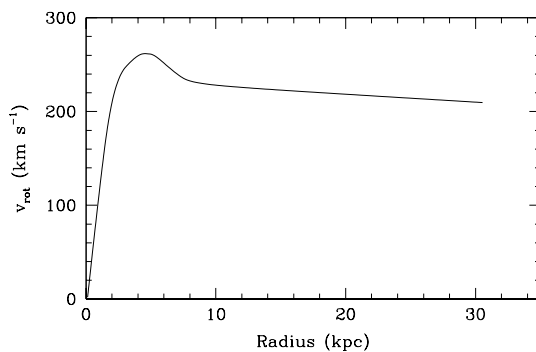


Figure 1: Basic rotation curve of a typical spiral galaxy, showing how the inner “solid body” curve changes to the outer curve at virtually constant velocity, passing through an intermediate zone with a flat maximum. This curve should follow the overall mass distribution within the galaxy.

out to a certain radius, r_c , followed by a virtually flat regime (almost constant value for v_r with r) from r_c out to very large radii. For a “standard” Milky Way mass galaxy r_c is of order a few kpc at which v_r attains a fairly flat maximum value v_{r_c} of between 200 and 250 km s⁻¹. At larger radii the value of v_r is almost constant at a value a little lower than v_{r_c} , out to radii of many tens of kpc; a sketch of this is given in Figure 1. The quasi-linear (“rigid body”) behaviour of the inner zone, and the quasi-constant behaviour of the outer zone of the rotation curve are the most standard observational characteristics of rotation curves, but although simple in form, they still defy comprehensive theoretical explanatory models. Of course the flat outer zone, whose great extent was measured in HI out to ten times beyond the limits marked by the stellar population, gave rise to the “missing mass” puzzle, which was a key step along the path to modern cosmologies.

When analyzing the observed two dimensional velocity field of a galaxy as projected onto the sky, taking into account that our observations always give only the

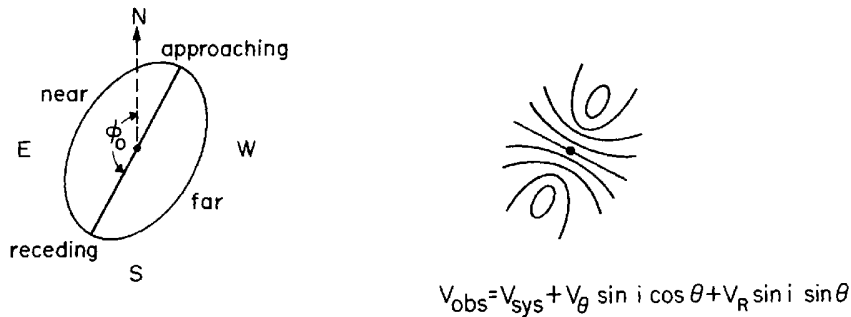


Figure 2: Schematic map of the “isovels” lines of constant observed radial velocity, which would be observed for a galaxy whose rotation curve measured along its major axis took the ideal form shown in Figure 1. This shows the form of the isovels which are subtracted from an observed two-dimensional velocity map of a galaxy, leaving residuals which give the non-circular velocity field.

radial component of velocity in the direction of the observer, we define the key parameters as: v_{sys} , the systemic velocity of the whole galaxy (i.e. its redshift); v_{θ} , the tangential velocity component in the plane of the galaxy, and v_r the radial component (with the initial assumption that there is no out of plane component); i is the angle of inclination between the galaxy and sky planes, and ϕ_0 the position angle of the galaxy major axis measured from north through east. With these definitions we can express the observed velocity v_{obs} at any point on the plane of the galaxy as seen projected onto the sky by:

$$v_{obs} = v_{sys} + v_{\theta} \sin i \cos \theta + v_R \sin i \sin \theta \quad (1)$$

where R and θ are the polar coordinates of a point $P'(R, \theta)$ in the plane of the galaxy, whose projection onto the plane of the sky is $P(r, \phi)$. These coordinates are related by:

$$\tan \theta = \tan(\phi - \phi_0) / \cos i \quad (2)$$

$$R = r \cos(\phi - \phi_0) / \cos \theta \quad (3)$$

In practice, as explained above, to simplify the analysis in order to get useful results from purely radially measured velocities, we first assume that radial velocities within the galaxy are small, setting v_R to zero. In this ideal purely rotating case, the resulting distribution of velocities radial to the observer will have a form given in Figure 2, where the lines drawn are termed “radial isovels”. The axis of symmetry of this

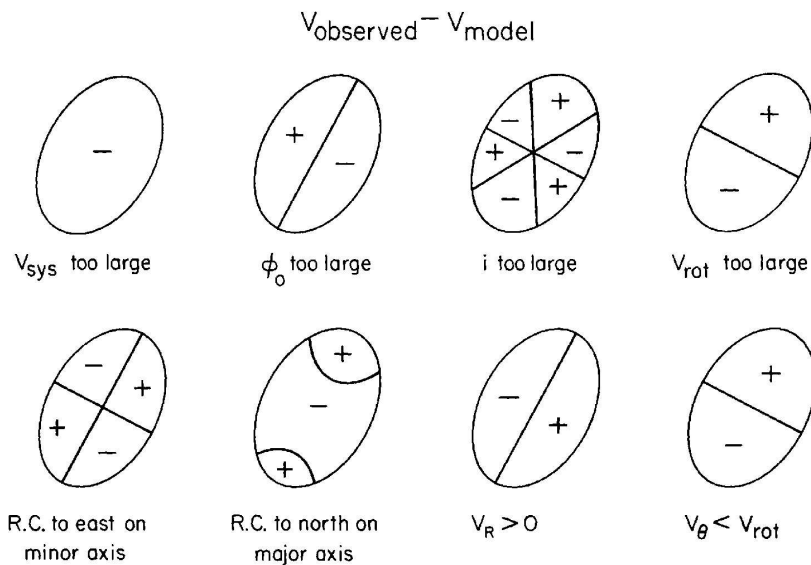


Figure 3: Schematic of systematic effects which may remain when a model two-dimensional rotation field is subtracted from an observed field in a spiral galaxy, when only one of the relevant parameters is badly selected or measured. From left to right and upper to lower panels: (a) Too large a systemic velocity chosen, (b) Position angle chosen for the analysis is too large, (c) The angle of inclination chosen is too large, (d) The rotation curve is scaled at too large a velocity, (e) The centre of rotation is to the east on the minor axis, (f) The centre of rotation is to the north on the major axis, (g) There is a positive expansion velocity, (h) There is a negative tangential velocity. Note that (a)-(e) represent measurement errors, while (f) and (g) imply true non-rotational velocity fields (in practice (d) and (g) are not easy to distinguish).

figure is the locus of maximum observed radial velocity, which should coincide with the major axis of the ellipse which defines the projected galaxy disc. The two implied methods of finding this axis, either from disc photometry or from velocity observations, should give indistinguishable results for a “well behaved” galaxy; measuring this axis yields the inclination angle i and position angle ϕ_0 for the later velocity analysis. Figure 2 shows the effect of projecting the rotation curve in Figure 1 into two dimensions and shows what we would expect to measure in a galaxy without radial or vertical motions. Any differences between this map and an observed map can then be

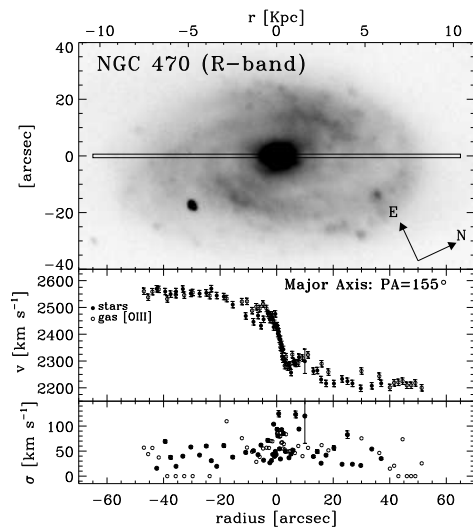


Figure 4: Major axis kinematic data for NGC 470, an Sbc galaxy, showing good coincidence between stellar and gas velocities, and low velocity dispersion even at the centre, as predicted for an object with little or no bulge concentration.

carefully analyzed to detect such motions. However one must be sure that the map itself gives correct values of a projected rotation curve. Some of the systematic errors possible which can be detected and corrected in this process are shown in Figure 3, where the assumption is made that a rotationally projected model rotation curve has been subtracted in two dimensions from the observational map. The diagram shows where positive and negative differences are found for different zones in the subtracted map for different types of bad adjustment between model and observations. We can see that some types of errors are best accounted for by systematic errors in the measurements of the systemic velocity, the major axis position angle, or the inclination angle, and others by an error in the position of the centre of rotation. However there are always possibilities of true non-circular velocity components, and as we will see later if the mass distribution within the galaxy suggests that such components should be present, it may be possible to measure them from the velocity field.

It is useful to point out here that when a spectral line measurement is made with the purpose of making a velocity map and extracting a rotation curve, if the spectral resolution is adequate one can derive the dispersion in the velocity of the stars or gas along the line of sight of the observation. In the basic case this dispersion is just measured as the full width at half maximum, or the Gaussian sigma, of the measured

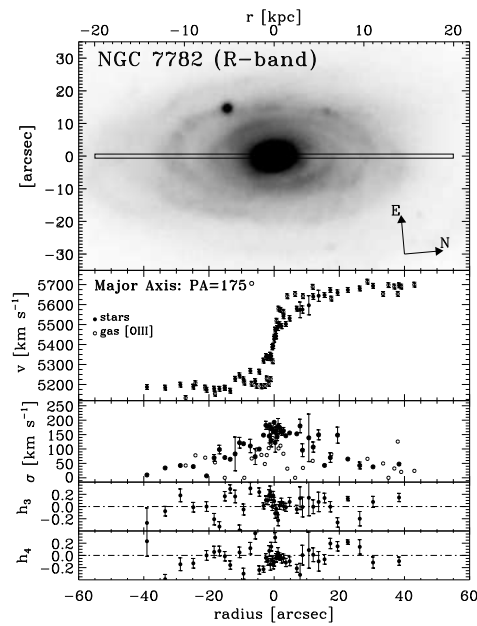


Figure 5: Major axis kinematics of NGC 7782 (Sb) showing how in the bulge the stars are supported against infall partly by pressure and partly by rotation, so their rotation velocities fall below those of the gas; also the stellar velocity dispersion is notably higher in the centre than that of NGC 470 in Figure 4.

line profile, either in absorption or in emission. To first order, the stars formed once the gas in a galaxy has settled into a disc will have a relatively low collective velocity dispersion, while the stars formed by gas in essentially radial collapse to form a bulge will have a relatively high dispersion. Typical values for the former are ~ 50 km s⁻¹ and for the latter are ~ 200 km s⁻¹. This difference may be used to help distinguish bulge from disc symmetry in a stellar component where this is not obvious from photometry alone, or even pick out a disc where this has previously been termed a bulge from photometric arguments ([7]). Since a stellar population or even a gas component, is supported against gravitational collapse by a combination of its axial rotation (circular motion) and its pressure (radial motion) we would expect to see zones with enhanced velocity dispersion having reduced rotational velocity, and vice versa, so the combination of velocity dispersion with rotation observations give complementary information on dynamic properties. It is also important to note that both emission lines from gas and absorption lines from stars can show multiple peaks

in their line of sight velocity distributions, and these can be interpreted as multiple population components, e.g. prograde and retrograde stellar motion, or strongly non-circular gas motion due to the presence of a bar. We will see some of these cases in the following sections.

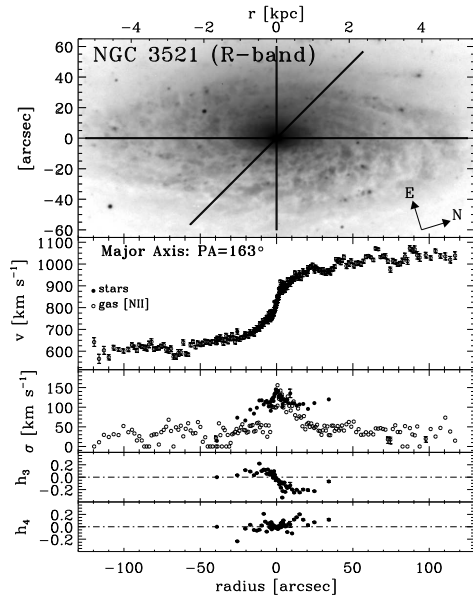


Figure 6: Major axis kinematics of NGC 3521 (Sb); here stars and gas rotate in unison, and the velocity dispersion in the centre is not high, in spite of the bulge. Note that the departures from zero of the symmetry parameter h_3 is a clue to a counter rotating component (see Figure 7).

3 Varied phenomenology in galactic rotation curves and velocity dispersions

There is considerable interest for dynamical and structural diagnostics in comparing the rotation curve measurements for stars and gas within the same galaxy. We will use here the rather rich sample presented completely in [9] and followed up in a number of relevant papers ([10], [11]; [8]). In late type galaxies, (Sc and later) the rotation curves measured using stellar absorption lines and gaseous emission lines are almost

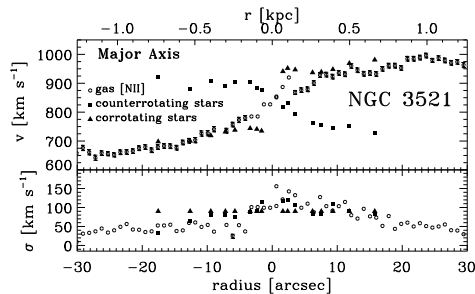


Figure 7: Result of gaussian decomposition of the spectra from which the kinematics of NGC 3521 (presented in Figure 6) were derived. This reveals a fraction of stars in counter rotation with the gas and the remaining stars in the bulge region, due either to a previous merger, or to the rotational properties of an end-on bar (see [8]).

always in excellent agreement, and the velocity dispersions of both components are relatively low. We will see that this is predicted for a system with a small or virtually absent central bulge. These results hold quite generally, except where the velocity and dispersion are measured close to a galactic bar, when deviations can occur. A good example of these properties is the kinematic information on NGC 470, in fact classified as Sbc, obtained with a long slit spectrum along its major axis, as shown in Figure 4 (from [12]). We can see good agreements between the rotation curves, and dispersion values in general below 100 km s^{-1} , which is low compared with values for galaxies with major bulges (see below). As well as the rising inner curve, and the near constant outer curve, we can see a sharp dip (symmetrical on either side of the centre) in velocity, followed by an oscillatory range, just outside 10 arcsec from the centre of the galaxy. This behaviour is what one would predict if the slit cuts zones of non-circular motion associated with the sides of a bar, and the presence of the bar is indeed seen well in the R-band image in Figure 4.

As we move to earlier type galaxies the gas and stars show diverging kinematic behaviour. This is essentially because a classical stellar bulge in any galaxy contains stars which are on “pressure supported” orbits, i.e. their orbits have strong radial velocity components, consistent with bulge formation by radial gravitational collapse of an initial gas cloud, or by near radial infall of captured material. Once a star has condensed out of a collapsing cloud, frictional dynamical processes are greatly reduced, so any effects tending to circularize orbits have extremely long timescales. Gas, on the other hand, always tends to relax into a plane perpendicular to the spin axis of the galaxy, and except in the presence of bars or other strongly non-axisymmetric components, into circular orbits. An excellent example is given by the

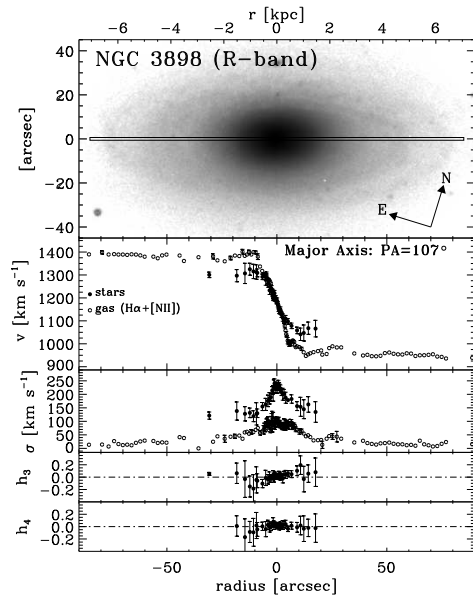


Figure 8: Major axis kinematic data for NGC 3898 (Sa), characteristic of galaxies with large bulges. The pressure supported stellar component shows much lower velocities, and much higher velocity dispersions in the bulge than does the gas.

Sb galaxy NGC 7782, in Figure 5 (from [12]) where the results of long slit spectroscopy along the major axis are shown. It is clear that in the inner zone where we can see an obvious bulge in the image, the stellar rotation curve falls well below the velocity of material in rotational equilibrium, which is well represented by the O III emission line rotation curve on the same diagram. While the gas is entirely supported by rotation, the stars are partly supported by “pressure” i.e. they have strong radial components in their orbits. This is well confirmed by the high value of the observed stellar velocity dispersion in the inner part of the galaxy, i.e. over 200 km s^{-1} . In the outer part of the rotation curve, corresponding to the exponential disc, the stellar curve rises and matches the gas curve very well, which is just what one would predict. A particularly interesting case is that of NGC 3521 shown in Figure 6 (from [12]). Here we have a case where the stars and gas apparently rotate in perfect unison, but the velocity curves have been obtained from long slit spectra, using only the velocities of the line peaks. However in Figure 6 we can see that the stellar spectral lines are far from symmetric, as shown by the behaviour of the line asymmetry parameter h_3 (for a description of the definitions of h_3 and h_4 , not used elsewhere in this paper,

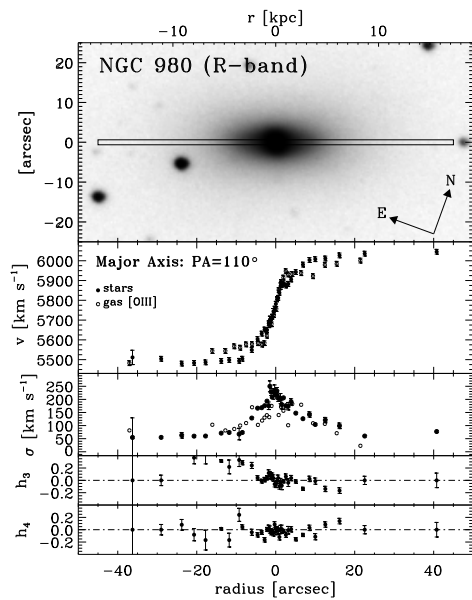


Figure 9: Major axis kinematic data for NGC 980, taken as a typical S0 galaxy. However the detailed analysis of the velocity dispersion and line symmetry parameters as functions of galactocentric radius, strongly suggests a rather small bulge embedded in a central disc plus a larger lens component, in interesting agreement with the conclusion of [7] that a significant fraction of S0's in fact have small bulges embedded in uniform discs, rather than large bulges as their classification would imply.

but appearing in the figures of this section, the reader is referred to [9]). A closer inspection of the lines reveals that they are double peaked, and when two gaussians are fitted, and new rotation curves plotted, we find an additional stellar rotation curve in the opposite sense to the first one, as seen in Figure 7. This counter rotating component could either be due to the acquisition of stars in a merger, or to the predicted phenomenon of a set of retrograde orbits within a bar ([13]). For further discussion of this case see [8], where it is suggested that an oscillatory pattern in the “flat” outer part of the rotation curve just beyond the steep inner rise, detected in a long slit spectrum from an angle intermediate between major and minor axes of the galaxy, indicates the presence of a bar. This bar must be virtually end on to us, and impossible to detect photometrically. This is an example of how the use of kinematics can enable us to detect, and often resolve structure in galaxies which is not detectable photometrically (see also [9]).

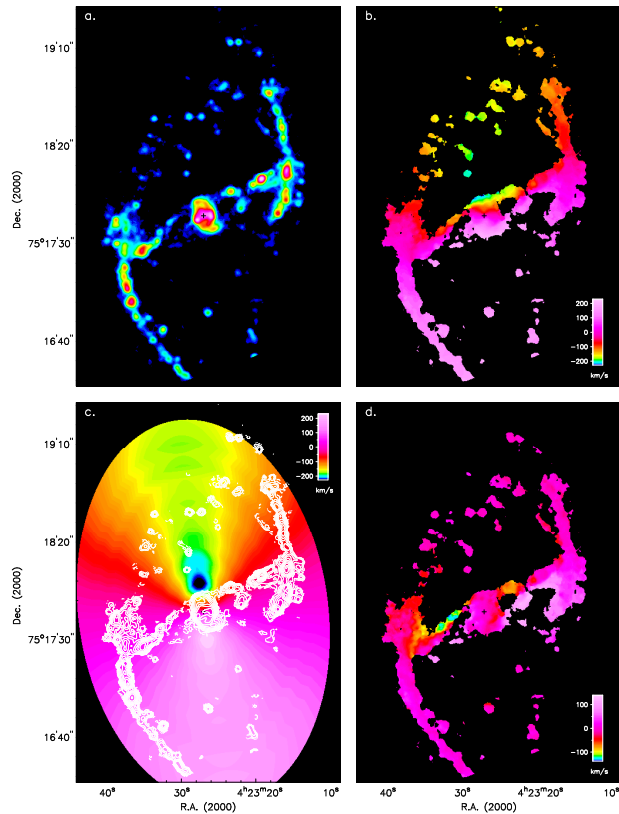


Figure 10: **a)** Intensity map (zeroth order moment) of the $H\alpha$ emission in NGC 1530. **b)** Velocity map (first moment) of the $H\alpha$ emission in NGC 1530. **c)** Model velocity map of NGC 1530, obtained from the $H\alpha$ rotation curve of the galaxy shown in Figure 11, with $H\alpha$ isointensity contours overlaid. We can clearly see “wiggles” at the radii of the spiral arms, due to the density wave streaming motions not subtracted off from the rotation curve. **d)** Map of the residual velocities of NGC 1530, obtained by subtracting the model velocity field (Figure 10c, after taking out the ripples due to the streaming motions in the spiral arms from the velocity map (Figure 10b).

The rotation curves and velocity dispersion curves for the gas and stars in the Sa

galaxy NGC 3898 are fairly characteristic of those for galaxies with major bulge components, but there is also evidence for an inner “thick, hot” disc as well as the normal outer disc. We can see this evidence in Figure 8 (from [12]), in which the curves have been derived from a long slit spectrum along the major axis of the galaxy. The stellar rotation curve falls well below that of the gas in the inner zone, as seen above for NGC 7782, and the velocity dispersion is very high in the centre, falling quite rapidly from 250 km s^{-1} to a plateau at $\sim 150 \text{ km s}^{-1}$; both types of behaviour are characteristic of the stars in a pressure supported bulge. The line shape parameters h_3 and h_4 show clear departures from zero, indicating the presence of more than one gaussian component in the stellar absorption lines. Close analysis of the individual lines ([10]) reveals that the lines come to us from a rapidly rotating disc superposed on a virtually non-rotating bulge. The separate hot disc is revealed by the plateau in the velocity dispersion of the stars between 12 arcsec and 25 arcsec from the centre of the galaxy, with a value of 110 km s^{-1} as shown in Figure 8. Beyond this, only the gas velocities can be well measured, and these show a very flat rotation curve with a very slowly declining velocity dispersion in the range $\sim 50 \text{ km s}^{-1}$, characteristic of normal galaxy discs. As an example of an S0 galaxy we have chosen NGC 980 because its kinematic differences between stars and gas are not very complex, for example it shows no evidence for counter-rotation, though many similar galaxies do show such evidence. The rotation curves and velocity dispersion curves for this galaxy are shown in Figure 9 (from [12]). The velocity dispersions of both gas and stars are high, $\sim 250 \text{ km s}^{-1}$ in the very centre, showing the presence of a dynamically hot bulge, but fall quite rapidly and are below 150 km s^{-1} at 5 arcsec radius. As for rotational velocity, the gas curve rises more rapidly than the stellar curve between 3 and 10 arcsec from the centre, which is normal for galaxies with bulge components. The stellar velocity shows a plateau, but at 10 arcsec the velocity of the gas dips below that of the stars, and remains lower out to some 20 arcsec, which is certainly unusual. If we look at the line asymmetry parameter h_3 it departs strongly from zero between 5 and 20 arcsec from the centre. [12] explains these features as due to an almost edge on disc component embedded in a more extended lens component, with a very compact luminous bulge with a 2 arcsec extent. This conclusion is in interesting agreement with that of [7] who showed, combining photometric and kinematic arguments, that a fair fraction of S0 galaxies have small bulges embedded in discs, rather than large bulges, as previously understood. The unusual behaviour of the gas rotation curve is explained as being due to a misalignment between gaseous and stellar components, and the whole system is modelled dynamically to fit the observed velocity and other line parameters. As the purpose of this article is to give an overview of the kinds of information which kinematic measurements provide, we will not go more deeply into these inferences here, but refer the reader to [10] and [12], to [8] and to [11], as well as to the most complete source, [9]. We must point out the general conclusion that even single slit rotation curves, obtained with high S:N ratio, high spectral and high spatial

resolution can offer us very powerful kinematic clues to the structure and dynamical history of galaxies, as illustrated here. Naturally two dimensional spectroscopy is in principle even more powerful, and we will describe one particularly interesting data set of this type here below.

4 The velocity field of the ionized gas in NGC 1530

As an excellent illustration of the use of a full two dimensional velocity field we take the case of the strongly barred galaxy NGC 1530 which we have mapped in velocity with a resolution of $\sim 15 \text{ km s}^{-1}$ and an angular resolution of $\sim 1 \text{ arcsec}$ across the full face of the galaxy using a scanning Fabry–Pérot, in $\text{H}\alpha$ emission. A detailed analysis of the kinematics and its implications for star formation (SF) can be found in [14]. Here we will stress some of the technicalities of the method and the types of information derivable which cannot be obtained using other methods. In Figure 10 we give a general display of how the observations give us information about the surface brightness and velocity distribution of the ionized gas in the galaxy. The original “data cube” gave a set of individual maps of the galaxy, each in a set narrow wavelength channel, of width $\sim 15 \text{ km s}^{-1}$ in this case. The analysis goes via a set of moment maps: the “zeroth” moment is the integrated surface brightness over all the channels, i.e. the full surface brightness of the galaxy in $\text{H}\alpha$ (Figure 10a), the first moment map (Figure 10b) is a two dimensional map of the local radial velocity, as dealt with theoretically in section 1, and the second moment map (not shown in Figure 10, but see [14]) is of the velocity dispersion in the ionized gas.

Here we concentrate on the first moment map which is essentially a map of the velocities of the peaks of the $\text{H}\alpha$ emission lines coming from all the pixels in the galaxy. The first step in its analysis gives us the rotation curve, and for NGC 1530 our first order measured rotation curve is shown in Figure 11. The fact that it is symmetric on either side of the centre of the galaxy suggests that we are not falling into any of the gross errors illustrated in Figure 3. However there are some subtle traps which we have not avoided, and which must be corrected in order to give a better plot of the true rotational velocity with radius. Within 5 arcsec of the centre there is a bump where the curve rises more steeply and then falls back to a linear regime, and between 40 and 100 arcsec there is a series of smaller bumps which differ from one side to the other, but with amplitudes well above the error bars. These outer bumps coincide in radius with the spiral arms and are due to non-circular motions associated with these streaming motions. Their amplitudes can be estimated by assuming that the mean matter distribution is radially smooth so that the true rotation curve is smooth. The differences between an interpolated smoothed curve and the observed curve in this range can be converted into amplitude estimates for the streaming motions, and are typically of between 10 and 40 km s^{-1} . This process is illustrated in Figure 12. In

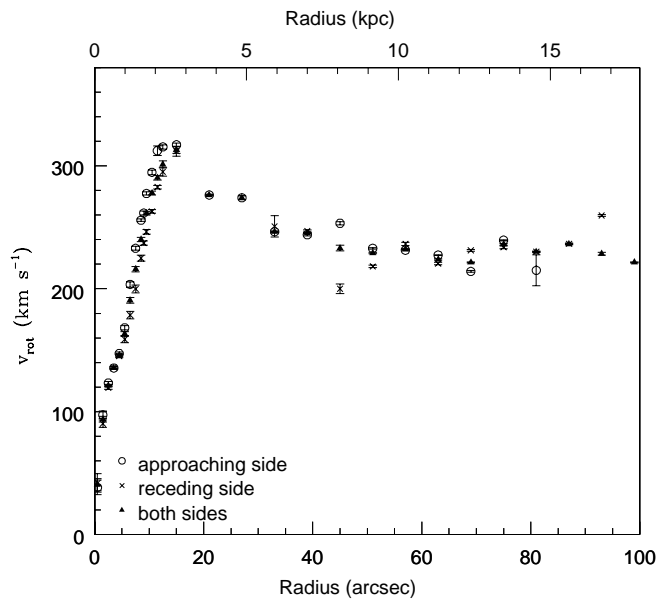


Figure 11: $H\alpha$ rotation curve of the disc of NGC 1530, for the receding and the approaching sides of the galaxy separately. The agreement between the two sides shows the symmetry of the velocity field and the reliability of the rotation centre.

Figure 10c we show the rotation curve projected into the plane of the sky to give a model which can then be subtracted from the original map, yielding a “residual” map of truly non-circular velocities. The presence of uncorrected streaming motions in this model is notable, and for detailed work on these motions we produced a corrected smoothed model.

The inner bump might be due to the presence of a small massive bulge or central bar but as we showed from HST imaging in the NIR in [14], no such massive features are in fact present. We therefore interpret this bulge as due to gas spiralling in towards the nucleus along interlocking tracks, a phenomenon predicted by [15], and observed clearly for the first time in this work, down to within 300 pc from the nucleus, a limit imposed by the resolution as NGC 1350 is not very nearby (~ 30 Mpc).

In Figure 10d we show the non-circular velocity field of NGC 1530. It is clear that we are detecting fast non-circular components, produced by the presence of the strong bar. Their presence is in fact detectable in the original velocity field, Figure 10b, and the skewed isovels in this figure are a classical illustration of the effects of a bar on

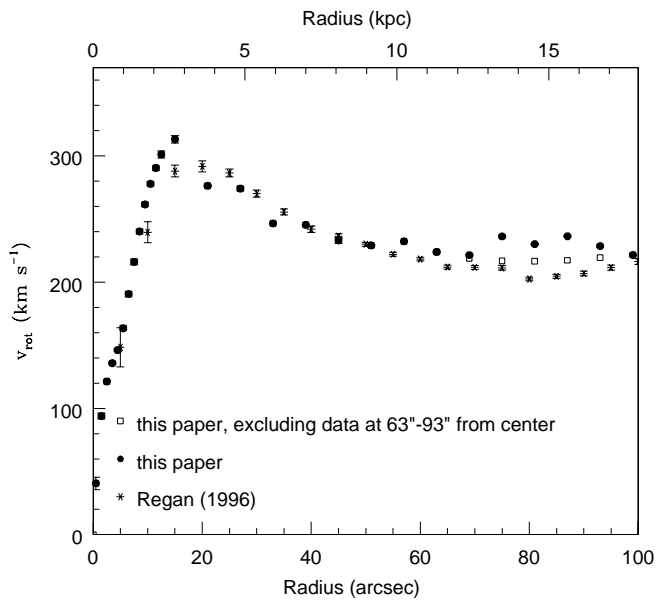


Figure 12: $H\alpha$ rotation curve of the disc of NGC 1530. This rotation curve has been obtained by subtracting the effect of the streaming motions in the spiral arms of the galaxy from the mean rotation curve shown in Figure 11.

the velocity field of a galaxy. This skew can be seen directly by comparing the field in Figure 10b with the idealized field in Figure 2, but in Figure 10d we have isolated the non-circular field, which can then be quantified. The amplitudes of these non-circular flows are well illustrated in Figure 13, with cross-sections perpendicular to the bar across the residual velocity map. The maximum amplitudes are found at some 20 arcsec from the nucleus, where the flows, in directions essentially parallel to the bar, stream past the bar in opposite directions at either side of it, with vector amplitudes of 100 km s^{-1} . These form a general field of gas flowing around the bar in quasi elliptical orbits, and exchanging angular momentum with the stellar mass of the bar where they form shocks as they approach its central axis, notably towards the ends of the bar in zones of high $H\alpha$ surface brightness.

A more graphic illustration of the power of this high resolution two-dimensional velocity mapping is given in Figure 14 where we have derived a map of the velocity gradients of the non-circular velocity components perpendicular to the bar direction. What is most striking is that the loci of maximum gradient along the bar trace

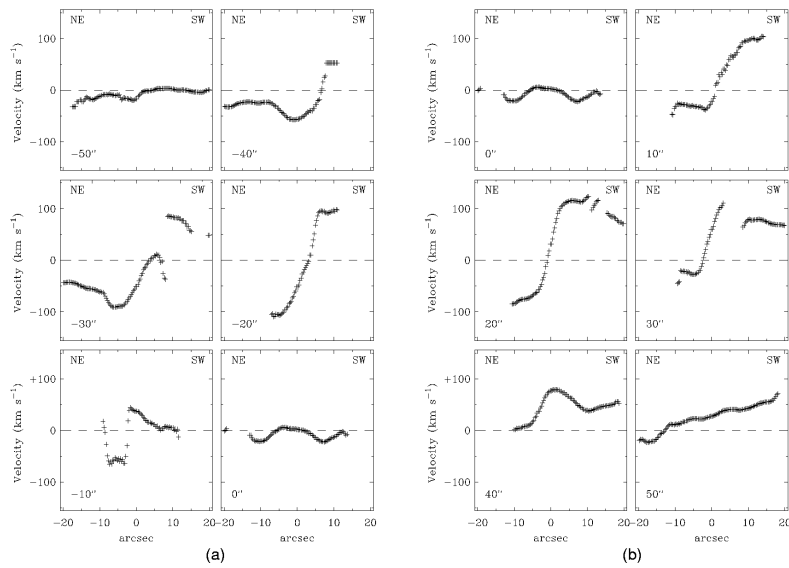


Figure 13: Profiles of the residual velocity perpendicular to the bar of the galaxy: to the SE (a) and to the NW (b). The distances of the profile tracks to the galaxy kinematic centre are indicated in the bottom-left hand corner of each plot.

perfectly the paths of the dust lanes (the only difference being that the velocity gradient map lacks complete continuity as the velocity measurements require local H α to be present in fair strength). This is because these loci, of maximum shear, are where the flow direction reverses, so the dust will tend to gather around these lines of low net velocity around the bar. Although this effect was predictable, this is the first detection and it tends to confirm what has become the classical theory of gas dynamics around bars ([16]). Further developments here will allow us to measure directly the net inflow rate of gas to the centre of galaxies like NGC 1530, giving valuable data to compare with models of how circumnuclear activity is fuelled in barred galaxies.

One very interesting general result of this kind of studies is the relation between velocities, velocity gradients and SF in the ISM. Figure 15(left) gives a plot of the H α surface brightness and the amplitude of the non-circular velocity field as functions of position on the bar of NGC 1530. We can see that there is a clear tendency for an anticorrelation between the two variables, i.e. high values of surface brightness correspond in general to low values of local non-circular velocity and vice versa. A

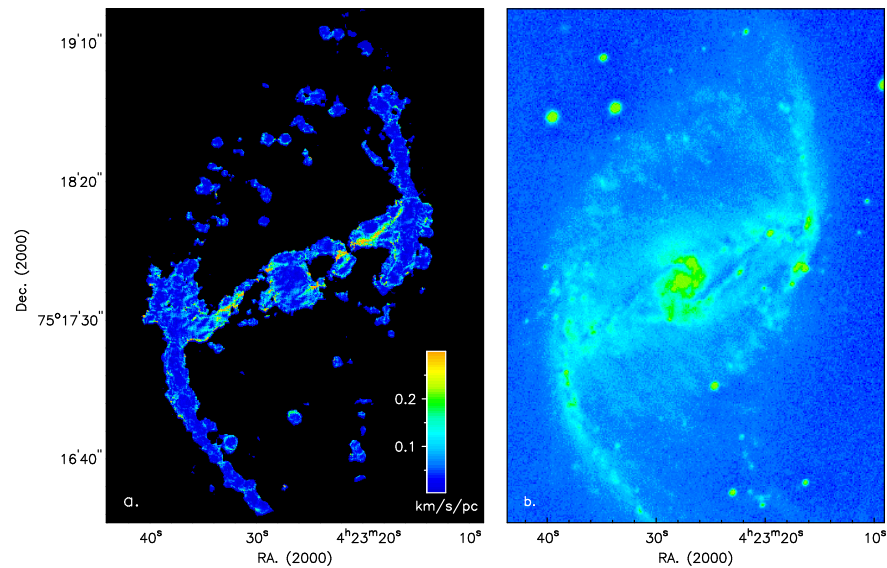


Figure 14: **a)** Velocity gradient map perpendicular to the bar. Zones of maximum shear are clearly seen (cf. the dust lanes in Figure 14b). **b)** Image of NGC 1530 in the optical V -band obtained with the KPNO 4-meter Mayall telescope.

quick inference from this would be that high local velocities act to inhibit SF. However we can go on to learn more by comparing the velocity gradient with the $H\alpha$ surface brightness, as shown in Figure 15(right). There is an even clearer anti-correlation between surface brightness and velocity gradient, and we can summarize by noting ([14]) that in the galaxy as a whole there are a few areas of high surface brightness which are in zones of high local non-circular velocity, but where the velocity gradient is low, whereas there are no high surface brightness areas where the velocity gradient is high. Thus the physical variable which best anti-correlates with local SF rate is non-circular velocity gradient, but in a direction perpendicular to the line of flow. We can explain this by understanding that high shear will tend to disrupt large gas clouds thus inhibiting SF. This qualitative conclusion deserves quantitative follow-up. It is also interesting that SF tends to occur at a small offset from zones of large velocity gradient perpendicular to the line of flow. This suggests that shocks which compress the gas are enhancing the local SF rate in these zones. There is a rather rich field to be explored here, given access to the relevant observing techniques.

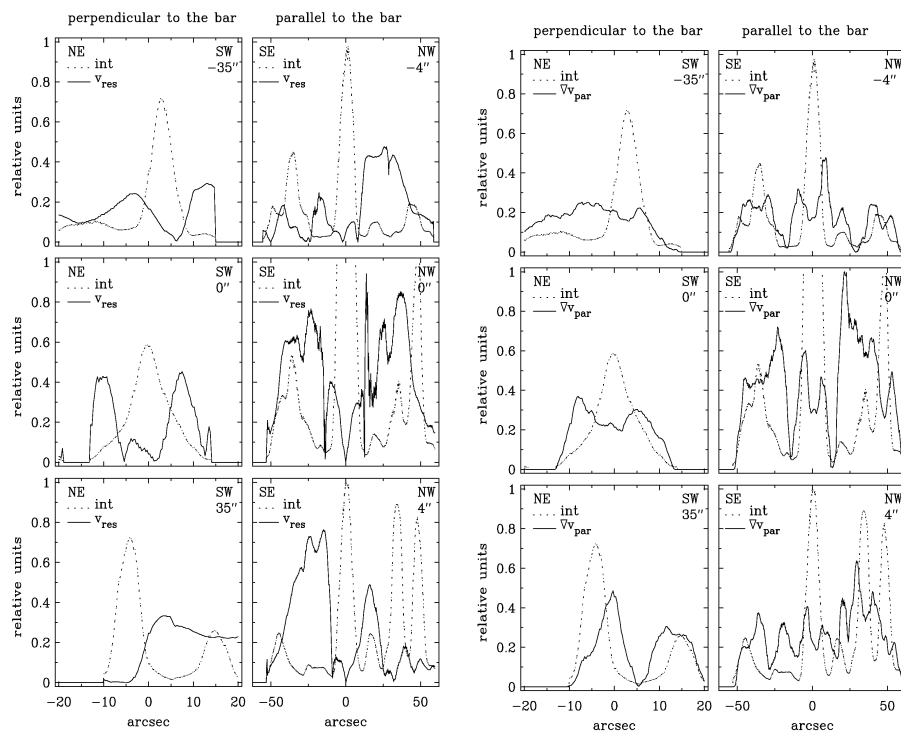


Figure 15: **(left)** Profiles of the normalized surface brightness in H α emission and residual velocity parallel and perpendicular to the bar. The distance of each profile track from the kinematic centre is indicated in the top right corner of each plot. **(right)** Profiles of the normalized H α surface brightness and residual velocity gradient parallel to the bar. The tracks of the profiles are the same as those in Figure 15(left).

5 Discussion: future kinematic observations

This article is designed to illustrate some of the inferences which can be made using kinematic mapping of galaxies, with emphasis on the rotation curve and departures from simple form, and the relationship of velocity to velocity dispersion where appropriate. While the use of HI has in the past given the most extensive coverage to this type of measurements, in the future we must use techniques which offer the best resolution and signal to noise as well as picking out the different structural components of galaxies. These include two dimensional optical and NIR spectroscopy

using fibre-fed systems, which have the advantage of simultaneous stellar and gas observations, but whose complete fields are small for the kinds of observations shown in section 3, and Fabry-Perot based systems, which can yield large fields at adequate spatial and spectral resolution, permitting rapid observing of complete galaxies, but which give us information in only one spectral emission line at a time, and coming from the relatively patchy emission of ionized regions. Both types of systems can be improved technically for the specific needs of kinematic mapping of galaxies. In the mid-term the use of ALMA in mapping the gas component via its molecular emission will certainly be an important boost for this line of investigation, which though now a mature method, will contribute much to our understanding of galaxies in the coming years.

References

- [1] Wolf, W. 1914, *Astronomische Nachrichten*, 199, 319
- [2] Pease, F.G. 1918, *Proc. Nat. Acad. Sci.*, 4, 21
- [3] Babcock, H.W. 1939, *Lick Obs. Bull.*, 498, 41
- [4] Rubin, V.C., Ford, W.K.Jr. 1970, *Astr. & Sp. Sc.*, 159, 379
- [5] van de Hulst, H.C., Raimond, E., van Woerden, H. 1957, *Bull. Astron. Neth.*, 14, 1
- [6] Blitz, L. 1975, *ApJL*, 231, 115
- [7] Erwin, P.E., Vega Beltrán, J.C., Graham, A., Beckman, J.E. 2003, *ApJ*, 597, 929
- [8] Zeilinger, W.W., Vega Beltrán, J.C., Rozas, M., Beckman, J.E., Pizzella, A., Corsini, E.M., Bertola, F. 2001, *Astr. & Sp. Sc.*, 276, 643
- [9] Vega Beltrán, J.C. 1999, PhD. Thesis, Universidad de La Laguna, Spain.
- [10] Vega Beltrán, J.C., Pignatelli, E., Zeilinger, W.W., Pizzella, A., Corsini, E.M., Bertola, F., Beckman, J.E. 2001a, *Astr. & Sp. Sc.*, 276, 509
- [11] Pignatelli, E., Corsini, E.M., Vega Beltrán, J.C., Scarlata, C., Pizzella, A., Funes, J.G., Zeilinger, W. W., Beckman, J.E., Bertola, F. 2001, *MNRAS*, 323, 188
- [12] Vega Beltrán, J.C., Pizzella, A., Corsini, E.M., Funes, J.G., Zeilinger, W.W., Beckman, J.E., Bertola, F. 2001b, *A&A*, 374, 394
- [13] Wozniak, H., Pfenninger, D. 1997, *A&A*, 317, 14
- [14] Zurita, A., Relaño, M., Beckman, J.E., Knapen, J.H. 2004, *A&A*, 413, 73
- [15] Englmaier, P., Shlosman, I. 2000, *ApJ*, 528, 677
- [16] Huntley, J.M., Sanders, R.H., Roberts, W.W.Jr. 1978, *ApJ*, 221, 521